ACADEMIC PRESS

Available online at www.sciencedirect.com
SCIENCE DIRECT®

Journal of Catalysis 216 (2003) 443–454

JOURNAL OF CATALYSIS

www.elsevier.com/locate/jcat

Nanostructured catalysts for NO_x storage–reduction and N_2O decomposition

Gabriele Centi,* G.E. Arena, and Siglinda Perathoner

Department of Industrial Chemistry and Engineering of Materials and European Laboratory for Catalysis and Surface Science (ELCASS), University of Messina, Messina, Italy

Received 8 July 2002; revised 10 September 2002; accepted 30 September 2002

Abstract

The concept of nanostructure is applied to catalysts for nitrogen oxide control and specifically in relation to the development of novel NO_x storage–reduction (NO_x SR) catalysts, as well as tuning metal particle size through metal–support interaction. In particular, the characteristics and reaction mechanism of Toyota-type NO_x SR catalysts are examined. Control of the nanostructure makes it possible to design samples with improved performance based on hydrotalcite starting materials. In Rh-on-zirconia catalysts for N_2O decomposition, the addition of small numbers of trivalent ions, inducing controlled oxygen vacancies in the zirconia support, allows the metal particle size to be tuned, thus promoting surface reactivity in N_2O decomposition even in the presence of two or three orders of magnitude higher concentrations of O_2 with respect to N_2O. The concept of controlling the nanostructure of the catalysts finds application in a wide range of situations of interest for catalytic technologies for environmental protection.

Keywords: NO_x; N_2O; Nanostructured catalyst; NO_x SR; Rh on zirconia; Hydrotalcite

1. Introduction

The use of catalytic technologies for protection of the environment has always been a major marketing area for catalysts, accounting for about one-third of sales (about $9 billion US in 2000), but historically it has been limited to a few major applications such as NO_x control (mobile and stationary sources) and sulfur and VOC abatement [1]. However, in the past decade the increasing necessity to reduce polluting emissions has stimulated the search for applications of catalysis to new areas [2]. Relevant examples are the development of new catalytic technologies for liquid waste treatment [3] and for greenhouse gas abatement or conversion [4]. Even in the case of established catalytic technologies, such as those for the treatment of emissions from mobile sources, new social requirements have renewed research efforts on several aspects:

(i) New catalysts for the abatement of NO_x in the presence of O_2 in lean burn or diesel engines (both engines characterized by reduced CO_2 emissions per km with respect to current gasoline engines working at a stoichiometric air to fuel ratio, but for which current three-way catalysts are not effective in reducing NO_x emissions below the levels required by law) [5];
(ii) Abatement of particulates from diesel engine emissions [6];
(iii) Ozone abatement;
(iv) Production of ultra-low-sulfur fuels [7].

Therefore, in the past decade social, environmental, and economic factors have been the driving forces for new or improved solid catalysts in the area of technologies for protection of the environment.

Differently from catalysts for chemical production and refining, catalysts in environmental protection applications often must operate under more extreme reaction conditions (very low or very high temperatures, in the presence of nonremovable poisons, with very high space velocities, with ultralow concentrations, etc.) and sometimes also must be able to operate efficiently with a range of different feeds or in the presence of fast changes in feed composition [8]. Minimizing the pressure drop is also often a critical aspect of catalyst properties. These challenging demands have

* Corresponding author.
E-mail address: centi@unime.it (G. Centi).

0021-9517/03/$ – see front matter
doi:10.1016/S0021-9517(02)00072-6

stimulated the search not only for more active or selective catalysts, but also for new catalytic materials:

- Having special stability characteristics (for example, resistance to hydrothermal treatments, to mechanical stress, and to the presence of plasmas or corrosive environments),
- Minimizing heat or mass transfer limitations, or
- Having a multifunctional behavior (for example, combining separation and reaction, or acting during sequential cycles in part as adsorbents and in part as catalysts).

In order to meet these requirements, research interest on these catalytic materials has been focused on both the molecular aspect (i.e., understanding the reaction mechanisms and structure–activity or selectivity relationships) and the overall catalyst structure, leading to the development of so-called structured catalysts (monoliths, membranes, fibers, and cloths) [9]. These catalytic materials were originally developed for environmental protection applications [10,11], but later their use was expanded to chemical processes.

Between this macroscale level of catalyst design/optimization and the molecular scale typical of reaction mechanisms on active sites, a third level of catalyst design has emerged in recent years as a critical factor in developing catalysts meeting the demanding characteristics necessary for environmental applications: the nanoscale level [12,13]. The various aspects involved in studies regarding the nanoscale level for solid catalysts can be summarized as follows:

(i) Control and tuning of the local environment around the active sites, in order to modify the diffusion and sorption characteristics of the reactants, products, or poisons of the reaction.
(ii) The architecture of active species at a nanoscale level, in order to optimize performances in multistep reactions or develop activity patterns in the catalyst which make it possible to optimize performance under a wider range of experimental conditions.
(iii) The nanostructure of the active species (size, structure, defects of nanosized oxides or metal particles). Nanosized particles often show novel reactivity properties, but the critical question is how to stabilize these nanosized particles during the catalytic reaction.
(iv) Long-range effects in catalysis, which include several aspects such as electron and ion bulk or surface transport, creation of defects and related dynamic reconstruction effects, particles to support interaction, and gas-to-solid interaction effects (accumulation of species on the catalyst, spillover of hydrogen or oxygen, bulk subsurface diffusion, etc.).
(v) Interface between different nanoparticles or nanoparticles and the support.

Some of these aspects are already well recognized in catalysis, while others have received less attention. The unifying aspect is the dimensional scale which determines the catalytic behavior. This may be viewed in other terms as the passage from the molecular scale of reaction at a catalytic site to the supramolecular level which considers how the environment around an active site determines the effective behavior of the active site.

2. Nanostructured NO_x storage–reduction catalysts

2.1. Background

Vehicles equipped with catalysts have been commercialized for over 20 years, but the growing number of vehicles in use (over 600 million worldwide) and increasing concerns about the global environment have created a demand to lower CO_2 emissions in addition to further reductions in CO, HC, and NO_x emissions. Current three-way catalysts require the engine to operate in a very narrow air to fuel (A/F) range near the stoichiometric value (A/F = 14.7), because only at that A/F value can CO, HC, and NO_x be removed simultaneously. However, at A/F = 14.7 the engine is not operating economically with regard to fuel consumption. Significant fuel economy can be obtained when the engine operates under lean conditions (A/F about 20–25), especially when diesel engines are used. The latter allow a potential fuel saving of about 30–35% compared to equivalent gasoline engines working near the stoichiometric A/F ratio, but the presence of O_2 in the emissions prevents current three-way catalysts (TWC) from efficiently reducing NO to N_2. Therefore, the objective of lowering noxious gas emissions (NO_x) (as required, for example, in the emission levels proposed by Tier 2 in the US and Euro V in Europe) together with greenhouse gas emissions (CO_2, N_2O) (objective of the Kyoto protocol) requires developing new catalytic solutions to selectively reduce NO to N_2 even in the presence of O_2.

One of the most advanced approaches is based on the NO_x storage–reduction (NO_xSR) concept originally developed by Toyota researchers [14–17]. These catalysts are based on the addition of BaO as the NO_x-storage component (about 15 wt%) to a Pt/alumina catalyst, but new generation catalysts also contain metal alkaline oxides to promote high-temperature behavior, TiO_2 nanoparticles to enhance regenerability, and Rh/ZrO_2 to promote in-situ generation of H_2 during periodic high-temperature (about 650 °C) regeneration [17]. Fundamental research on NO_xSR catalysts [18–23], however, has been limited to the study of Pt–Ba/alumina materials.

The principle of operation of these catalysts is based on a periodic change in the composition of the exhaust gases of the engine from lean (excess air) to rich (excess fuel) conditions by special engine management. During the longer lean period NO is oxidized to NO_2 and stored on the catalyst in the form of nitrates, which are reduced to nitrogen during the subsequent rich period. Since the nitrate reduction rate is much faster than the rate of surface NO_x storage (around two

orders of magnitude), a net saving of fuel is possible. Such catalysts are a good example of nanostructured catalysts having different functionalities: (i) the Pt for oxidation of NO during the lean period and reduction of nitrate during rich period, (ii) the alkaline or alkaline-earth oxide as an NO_x storage element, (iii) the oxide support to maintain high dispersion of the noble metal and NO_x storage component, and (iv) the other components (titania, Rh/ZrO_2) to promote regenerability.

To meet the need for (i) a continuous transfer of oxidized NO_x species from the metal to the storage component during the lean period and back during the rich period and (ii) fast processes (rich spikes are in the few hundred milliseconds range), the nanostructure of the catalyst is a key aspect to improve catalyst performance. In particular, a close interaction between the Pt particles and the NO_x storage component is necessary, but on the other hand the contact between the Pt particles and the metal alkaline-earth oxide (BaO) deactivates the Pt oxidation activity by an electronic effect [14,15]. This causes lowering of the activity at low temperature (below 250 °C), a critical problem especially for emissions from light-duty diesel engines, since a large part of the testing cycle is characterized by low-temperature emissions, typically in the range 120–200 °C.

2.2. Nature of active species and reaction mechanism

The effective NO_x storage component is not BaO, but $BaCO_3$ spread over the support. Temperature-programmed desorption tests on $BaCO_3$ supported on alumina evidence two decomposition temperatures with formation of gaseous CO_2, the first very broad in the 250–600 °C temperature range (with a shoulder near 350 °C) and the second at higher temperatures (630–720 °C temperature range) (Fig. 1a), corresponding to decomposition on noncrystalline and crystalline $BaCO_3$, as confirmed by high-temperature XRD data. The total amount of $BaCO_3$ detected on samples equilibrated at room temperature in air nearly corresponds to the nominal amount of BaO (Fig. 1b), although it is always slightly lower and considerably deviates for amounts of BaO higher than about 15 wt%, due to the presence of crystalline BaO as detected by X-ray diffraction analysis. Above about 15 wt% the higher temperature desorption peak (above 600 °C) also becomes relevant.

Reported in Fig. 1c is the mean NO_x conversion observed during the lean period in these samples. The NO_x conversion changes during each period with a lean composition (2 min), because the NO_x storage capacity of the catalyst is progressively saturated. The NO_x conversion is thus averaged over the lean period. Furthermore, the value is averaged over several cycles in order to obtain more reproducible data. The maximum conversion of NO_x is observed in the range 300–400 °C, because at lower temperatures the effectiveness is limited by the rate of NO oxidation to NO_2, and at higher temperatures by the stability of the nitrate species over the catalyst. However, the nature of the barium compounds also

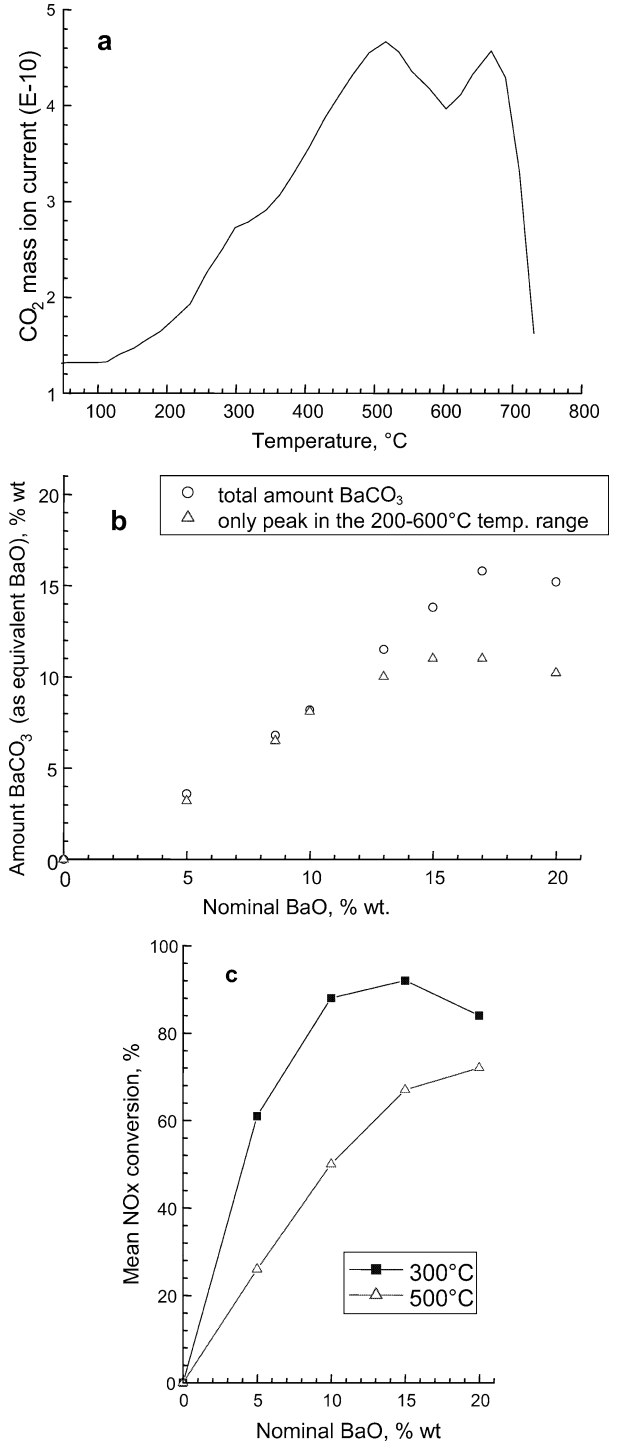

Fig. 1. (a) Formation of CO_2 during temperature-programmed desorption (ramp 10 °C/min) experiments with 20 wt% $BaCO_3$ on γ-Al_2O_3 (100 m^2/g) sample. (b) Amount of $BaCO_3$ determinated (as equivalent BaO wt%) during temperature programmed desorption experiments on Pt (1 wt%)–BaO/γ-Al_2O_3 catalysts with different nominal composition in terms of BaO loading: total amount of $BaCO_3$ and single peak in the 200–600 °C temperature range. (c) Mean NO_x conversion at 300 and 500 °C during the lean period in a sequence of 20 lean–rich composition cycles as a function of the nominal BaO loading in Pt (1 wt%)–BaO/γ-Al_2O_3 catalysts. Lean period composition: 0.1% NO, 5% O_2, 10% CO_2, remainder He for 120 s. Rich period composition: 2% H_2, 10% CO_2 in He, 5 s. Space velocity: 48,000 h^{-1}.

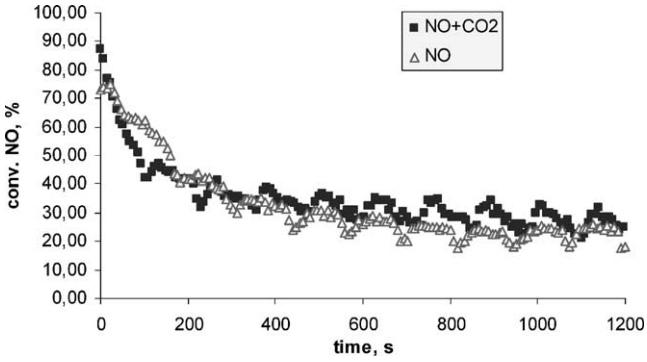

Fig. 2. NO_x conversion on a Pt (1%)–BaO (15%)/Al_2O_3 catalyst at 300 °C during a sequence of cycles in lean–rich conditions and in the presence or absence of 11% CO_2 in the feed. Lean period composition: 5% O_2, 10.8% (or 0%) CO_2, 954 ppm NO, remainder He; 120 s. Rich period composition: 3.3% CO, 1.1% H_2, 6000 ppm C_3H_6, 5% O_2, 10.8% CO_2, 954 ppm NO, remainder He; 0.2 s.

affects performance. At 500 °C, good correlation is observed between total amount of $BaCO_3$ on the catalyst (Fig. 1b) and mean NO_x conversion (Fig. 1c). However, at a lower temperature (300 °C) the correlation is instead observed with the amount of $BaCO_3$ present in the lower temperature broad peak (temperature range) (200–600 °C) and attributed to the $BaCO_3$ spread over the alumina surface. This is in agreement with other literature data [24] indicating that over the catalytic surface, the well-dispersed barium phase can play an important role in the NO_x trapping properties of these catalysts. Crystalline BaO plays a minor role in determining NO_x storage performance, because due to the expansion of the crystalline unit cell in passing from BaO to $Ba(NO_3)_2$, immediately after formation of the first adsorption layers the rate of accumulation becomes governed by bulk diffusion, a process too slow to contribute significantly to the behavior of these catalysts in practical conditions of reaction.

NO, after being oxidized to NO_2 over the Pt (a fast process at temperatures above about 250 °C), reacts with the Ba carbonate, forming CO_2 and Ba nitrate. The mechanism, however, is more complex, as indicated by the fact that CO_2, even in large amounts (typically around 11% in the exhaust from motor vehicle engines), does not have a major effect on the NO_x storage capacity of the catalyst, even if the NO concentration is around 100 times lower than that of the CO_2. Figure 2 shows that similar behavior is observed independent of the presence of CO_2 during the lean period. It should be noted that in these tests, in order to better analyze the behavior of the more active species, the regeneration period in rich conditions was quite short and thus only the more reactive nitrate species could be reduced. Therefore, the fresh sample initially loses activity during the first 5–6 cycles of 120 s each, but then the activity becomes constant.

If the reactivity of the catalyst in NO_x storage is determined from the equilibrium between carbonate and nitrate surface compounds, a considerable influence of the presence of CO_2 in the feed can be expected, different from that observed. On the other hand, Ba carbonate is relatively thermally stable on alumina, as indicated in Fig. 1a. Indeed, the thermal stability is not significantly different from that of supported Ba nitrate.

In situ DRIFT experiments (Fig. 3, left graph) evidence that immediately after the addition of the NO + O_2 feed, nitrites (M–O–NO) form (band at 1206 cm^{-1}), but these species quickly transform into mono- (M–O–NO_2) and bidentate (M–2O–NO) nitrates (1322 and 1535 cm^{-1}) [25]. No further changes occur with increasing time on stream, apart from an increase in the intensity of the bands. However, the spectrum is affected by negative bands which develop at the same time in the region around 1400 cm^{-1}, due to the transformation of Ba carbonate to Ba nitrate and the evolution of CO_2, which can be monitored in the

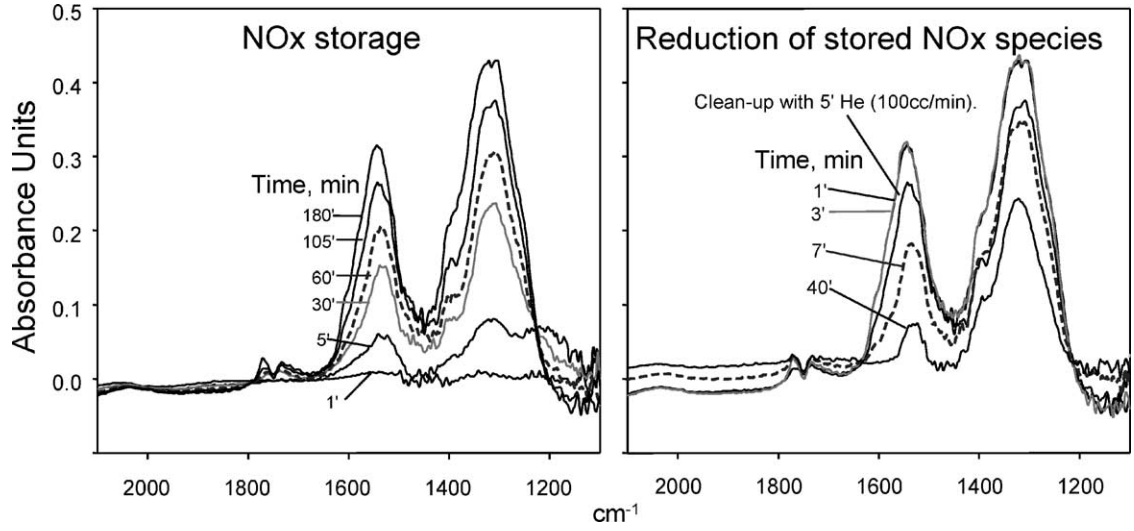

Fig. 3. In situ DRIFT experiments of the process of accumulation of NO_x species over a Pt (1%)–BaO (15%)/Al_2O_3 catalyst (350 °C, flow of 0.1% NO, 0.8% O_2 in He) (left graph) and subsequent reduction at the same temperature (flow of 0.6% H_2 in He) (right graph). The time in the figure for the different curves indicates the time in minutes after the switch from a pure He feed to the mixture indicated above.

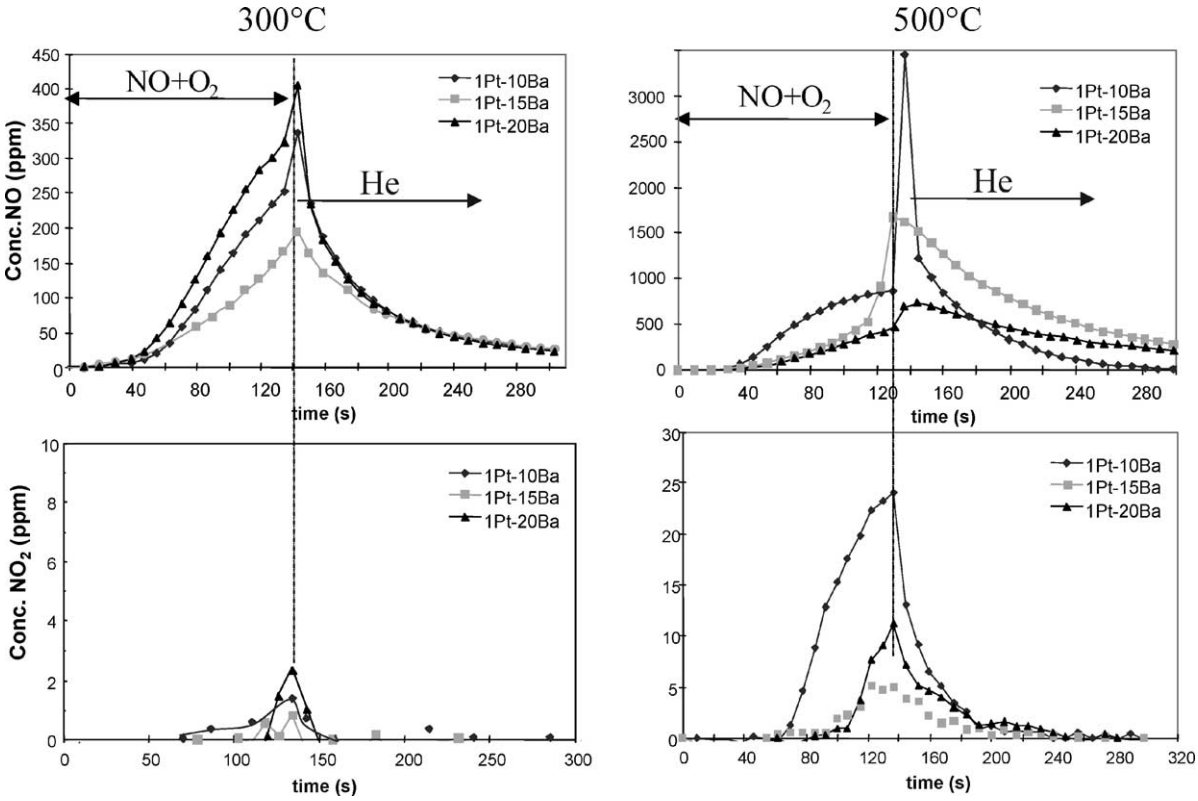

Fig. 4. Transient reactivity experiment on Pt (1%)–Ba (10–20%)/Al_2O_3 catalysts (10 wt% BaO: 1Pt–10Ba; 15 wt% BaO: 1Pt–15Ba; 20 wt% BaO: 1Pt–20Ba) at 300 and 500 °C: change in the concentration of NO (upper graphs) and NO_2 (lower graphs) as a function of time during a rectangular pulse of NO + O_2 (0.1% NO, 1% O_2 in helium) followed by a flow of pure helium.

gas phase. Indeed, when the surface carbonates are fully removed from the catalyst by treatment at temperatures above 500 °C, a further intense band is noted centered at 1413 cm^{-1}, indicating the presence of monodentate nitro (M–NO_2) compounds. The subsequent reduction of this sample with H_2 (Fig. 3, right) gave rise to a decrease in the intensity of the bands associated with nitrates, but no other changes are noted, indicating that the reduction occurs without intermediate formation of nitrites or adsorbed NO_2. Varying the reaction temperature or contacting the catalyst with NO_2 only did not provide markedly different results.

Further indication of the nature and stability of NO_x species was obtained from transient reactivity rectangular pulse experiments (Fig. 4). In these tests, the catalyst reactivity was monitored during sequences of rectangular variations in the concentration of the reagents, but CO_2 was not cofed in order to monitor all nitrogen oxides. Figure 4 shows the NO conversion and the formation of NO_2 on three 1%Pt–BaO/Al_2O_3 samples with increasing amounts of BaO from 10 to 20%. The graphs on the left refer to a reaction temperature of 300 °C, and the graphs on the right to a reaction temperature of 500 °C. During the 140 s of the rectangular pulse of NO + O_2, the conversion of NO is initially complete (no NO in the reactor outlet), and then decreases. The sample with lower residual NO is that with the intermediate amount of BaO, in agreement with the data in Fig. 1. Only traces of NO_2 are detected at 300 °C at the end of this rectangular pulse (1–2 ppm), which immediately stops after shutting down the NO + O_2 feed. However, completely different behavior is found for NO. Immediately after the NO + O_2 feed is shut down there is an overshoot in the concentration of NO, which then slowly decreases to zero. The trend is similar for all three catalysts with increasing amounts of BaO. At 500 °C a similar trend is observed, but in this case the most active sample is that with the highest amount of BaO. The sample with the lowest amount of BaO (1Pt–10Ba) becomes saturated more quickly and a much higher amount of NO_2 (up to 25 ppm) forms. This suggests that well-dispersed Ba carbonate reacts faster with NO_2 (formed by oxidation on Pt), and other Ba compounds (crystalline Ba carbonate and BaO) react slower, but form nitrate species that are more stable at higher temperature. For this reason, at higher temperatures 1Pt–20Ba shows better behavior than 1Pt–15Ba. This differs from the results at lower temperatures, in good agreement with the indications from Fig. 1.

Also, at 500 °C, the formation of NO_2 drops to zero quickly after the NO + O_2 feed has been stopped, while NO formation shows a large overshoot immediately after the feed has been switched from NO + O_2 to He, and then slowly decreases to zero. If the desorption of NO_x is determined by a surface equilibrium, no overshoot is expected and a different trend of the desorption of NO and NO_2 is expected. This suggests that part of the adsorbed NO_x is present as a

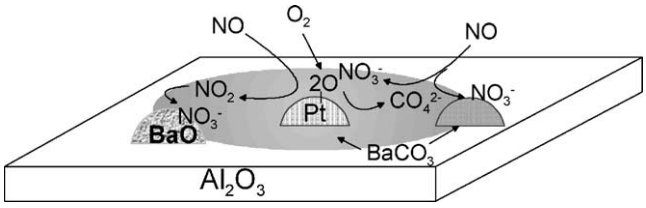

Fig. 5. Proposed mechanistic scheme for NO_x storage during lean conditions and presence of CO_2 in the feed.

weak $NO \cdot O_x$ surface complex. Probably the O_x species are spillover oxygen generated by interaction of O_2 with Pt and form peroxocarbonate by reaction with carbonate. They are dynamically formed when O_2 is present in the gas phase, but when the O_2 concentration stops their concentration progressively decreases and NO desorbs from the catalyst surface. The mechanism (see Fig. 5 for a schematic drawing) is thus of dissociation of O_2 over Pt to generate atomic oxygen, which may react either directly with NO to form nitrite and later nitrate or with carbonate species to form peroxocarbonate, which then oxidize NO, forming a $NO \cdot O_x$ surface complex stabilized by Ba. The hypothesis is not in contrast with IR data, because the bands observed in infrared spectroscopy (see Fig. 3) are quite broad and the bands for the $NO \cdot O_x$ surface complex are expected in the same region. The two pathways of reaction coexist during catalytic tests, but the predominance of one pathway over the other depends on the presence and concentration of CO_2 in the feed. This hypothesis should be further examined; however, it does explain why the behavior of these catalysts cannot be explained on the basis of only an equilibrium between carbonate and nitrate Ba surface compounds.

The reaction mechanism is consistent with other literature data. Schmitz and Baird [26] also observed that nitrate formation may occur via oxidation of surface adsorbed species and not only over noble metal surface. Paterson et al. [27] found that spillover of activated oxygen and/or an activated form of NO_2 may be required for the storage step and for the samples to behave as effective storage materials. Prinetto et al. [28] argued for the possible formation of Ba oxycarbonate. Other authors [29] instead indicate that CO_2 has a marked inhibiting effect on the storage of NO_x and BaO is the active species. However, this is in contrast with other results, as shown below.

2.3. The question of hydrothermal stability

An important characteristic of NO_x storage–reduction catalysts is their hydrothermal stability, because the temperature of the catalyst during full loading operations may reach temperatures above 650–700 °C and the steam concentration in the emissions is around 10%. A typical test to check hydrothermal stability of these catalysts is to analyze the mean NO_x conversion (as reported before, the mean NO_x conversion during a single period in lean conditions, which is further averaged over a series of lean–rich cycles) as a function of the reaction temperature before and after treatment of the catalyst under hydrothermal conditions (typically at 800 °C for several hours using humidified air). Reported in Fig. 6 (upper graph) are the X-ray diffraction patterns of the Pt (1 wt%)–BaO (15 wt%)/alumina sample calcined at 650 °C before (A) and after (B) the hydrothermal treatment. In the sample before the hydrothermal treatment, together with the reflections of alumina, there are sharp and intense reflections for $BaCO_3$, together with less intense and broader reflections for BaO. After hydrothermal treatment, the reflections for $BaCO_3$ completely disappear, while those for BaO increase in intensity and become sharper. The XRD reflections of $BaCO_3$ were not observed in the sample after hydrothermal treatment and further catalytic tests, even though the concentration of CO_2 in the feed was about 11%. $BaCO_3$ is probably present at least in part as a well-spread XRD undetectable compound, but the decrease of the sharp reflections of crystalline $BaCO_3$ and the parallel increase of those of crystalline BaO indicates that retransformation of crystalline BaO to $BaCO_3$ is not a fast process. The transfor-

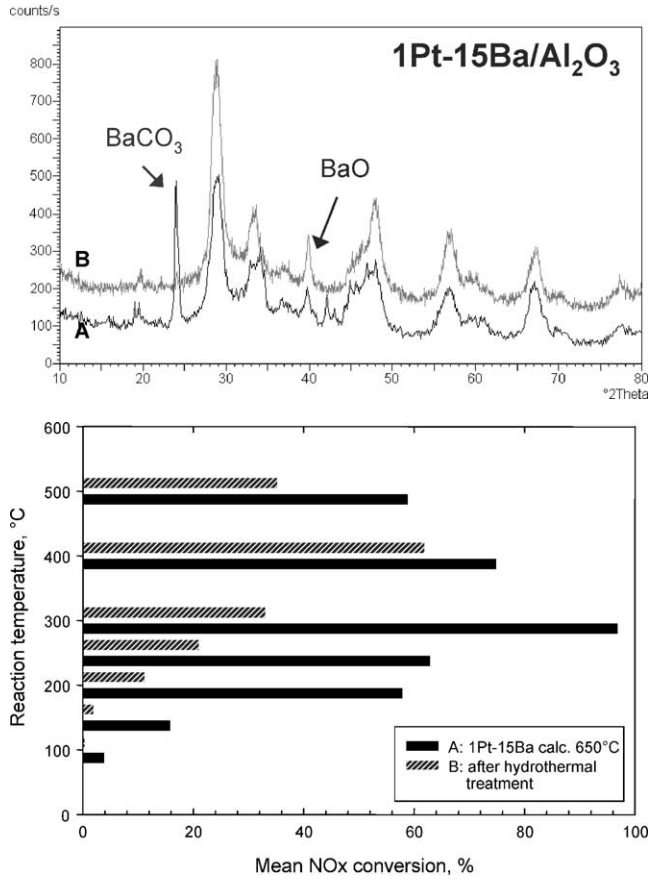

Fig. 6. Lower graph: effect of the reaction temperature on the NO_x mean conversion (over 20 cycles) of 1Pt–15Ba/Al_2O_3 calcined at 650 °C, before (A) and after (B) hydrothermal treatment at 800 °C (24 h, 3% H_2O in air). Lean period: 120 s, 5% O_2, 10.8% CO_2, 954 ppm NO, remainder He. Rich period: 6 s, 3.3% CO, 1.1% H_2, 6000 ppm C_3H_6, 5% O_2, 10.8% CO_2, 954 ppm NO, remainder He. 20,000 h^{-1}. Upper graph: X-ray diffraction patterns of the same A and B samples before the catalytic tests. No relevant changes are noted after the catalytic reaction.

mation is reversible, but requires longer times. In fact, when the sample is left in open air for a long time and analyzed again, the reflections of $BaCO_3$ are detected again.

The reactivity in NO_x storage markedly changes after hydrothermal treatment (Fig. 6, lower graph). The activity at temperatures lower than about 350 °C decreases to values of about one-third of the original value and the maximum in activity shifts from about 300 °C to 400 °C. This confirms previous indications that at temperatures around 300 °C Ba carbonate is the species which reacts faster with NO_x, while at higher temperatures BaO plays a major role, essentially due to the higher thermal stability of the nitrate formed on it.

2.4. Reaction mechanism, nanostructure and catalyst design

Can the above discussed reaction mechanism be used to design new improved catalysts having better hydrothermal stability? There are some recent indications of this possibility [30,31] using novel NO_x storage–reduction catalysts based on Mg–Al hydrotalcite precursors.

Hydrotalcite anionic clays (HTs) are characterized by positively charged two-dimensional sheets with water and exchangeable charge-compensating anions in the interlayer region [32]. The general formula is

$$\left[M^{2+}_{1-x}M^{3+}_{x}(OH)_2\right]^{x+} - \left(A^{n-}_{x/n}\right)\cdot mH_2O, \qquad (1)$$

where M^{2+} and M^{3+} represent divalent and trivalent cations in the brucite-type layers. Although various divalent and trivalent cations can be introduced, the most common, present also in the mineral hydrotalcite, are magnesium and aluminum, whereas the anions are carbonate groups, e.g., $Mg_6Al_2(OH)_{16}CO_3\cdot 4H_2O$. The HT structure closely resembles that of brucite, $Mg(OH)_2$. In brucite, magnesium cations are octahedrally coordinated by hydroxyl ions, giving rise to edge-shared layers of octahedra. In HT, part of the Mg^{2+} ions is replaced by Al^{3+} ions, resulting in positively charged cation layers. Charge-balancing anions (usually $CO_3{}^{2-}$) and water molecules are situated in the interlayer spaces between the stacked brucite-like cation layers.

At temperatures around 650 °C hydrotalcite transforms to a MgO-type mixed oxide having small MgO or $MgCO_3$ particles supported on the Mg–Al mixed oxide. The latter transforms to a spinel-like phase at temperatures around 900 °C.

The interesting characteristic of HT-derived materials as NO_x storage–reduction catalysts is the formation of well-dispersed MgO particles which can act as NO_x storage components. The characteristics of these materials depend on the Mg/Al ratio and the presence of other elements in the structure [32], properties which can be easily altered. A further characteristic of these materials is the possibility of reconstructing the HT structure during catalytic reaction due to the "memory effect" in the Mg(Al)O mixed oxides [32,33], especially in the presence of the high water and CO_2 concentrations typical of emissions from car engines. This "memory effect" originates from the fact that atoms in the heat-treated HT more or less retain their original positions, making reconstruction of the HT structure possible.

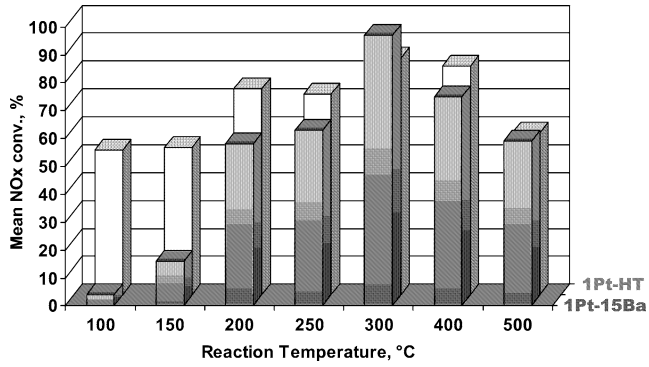

Fig. 7. Comparison of the mean NO_x conversion as a function of the reaction temperature during NO_x storage–reduction tests on fresh Pt (1%)–Ba (15%)/Al_2O_3 catalysts (1Pt–15Ba) and Pt(1%)–HT catalysts, where HT indicates a hydrotalcite starting material having a Mg^{2+}/Al^{3+} ratio of 66:34. Experimental conditions as in Fig. 6.

According to the previous discussion of the reaction mechanism and reactivity of the different Ba surface compounds, it is necessary to keep the Ba well dispersed on the catalyst surface and avoid sintering of the BaO particles. The "memory effect" present in materials derived from HT allows a dynamic effect of reconstruction of HT and its decomposition during catalytic reaction, which in principle make it possible to maintain well-dispersed Ba surface compounds and limit their sintering. This mechanism should especially promote low-temperature activity. In agreement, comparison of the performances of a Toyota-like catalyst (1Pt–15Ba) with that of the sample derived from a Mg/Al hydrotalcite precursor (Mg^{2+}/Al^{3+} ratio = 66:34) (Fig. 7) indicates an effective promotion of the low-temperature activity, a relevant aspect especially for light-duty diesel engine applications, as indicated previously.

After hydrothermal treatment the behavior of 1Pt–HT catalyst is analogous to that of the 1Pt–15Ba sample (considerable deactivation), in apparent contrast to the expected stabilization effect due to dynamic reconstruction/decomposition of the HT structure [32]. Characterization of the sample after hydrothermal treatment [32] indicated significant sintering of the Pt particles, which causes a lowering of the NO_x storage–reduction performance due to a decrease in the rate of NO oxidation and/or generation of spillover oxygen. Therefore, on HT-derived samples it is necessary to improve stability against sintering of the noble metal. One possibility is to add a compound such as copper which forms an alloy with Pt and limits its sintering.

The 1Pt–Cu/HT was prepared in the same way as the 1Pt–HT discussed above, but before Pt was loaded using a $Pt(NH_3)_2(NO_2)_2$ precursor, the HT support was impregnated with an aqueous solution containing $Cu(NO_3)_2\cdot 3H_2O$, in order to have a loading of copper equivalent to

4 wt% as CuO. After calcination at 550 °C, Pt was then added and the sample further calcined [32].

The nature of the Pt phase and the influence of copper on its properties were analyzed by CO chemisorption on samples that were either oxidized or reduced at 350 °C with H_2 [32]. On the 1Pt–Cu/HT prereduced sample the band due to CO linearly bonded on Pt shows a red shift (from 2065 to 2010 cm^{-1}) with respect to those in Pt/HT, while a blue shift (from 2108 to 2116 cm^{-1}) was observed for the band of CO chemisorbed on $Cu^{\delta+}$ sites with respect to the Cu/HT samples. These findings indicate that electron transfer from Cu to Pt atoms occurs, thus increasing the σ donation from CO to Cu and the π back-donation from Pt to CO. Similar behavior has been observed for alumina- and silica-supported Pt–Cu catalysts and ascribed to the formation of Pt, Cu alloys [34]. As expected, due to the high Cu/Pt atomic ratio in the Pt–Cu/HT samples (Cu/Pt = 12), the effect of the charge transfer is larger on the Pt than on the Cu carbonyls. The band of the Pt carbonyls also has a lower intensity than on the Pt/HT samples. This can be ascribed to the diffusion of a part of the Pt from the surface to the bulk of the copper particles during the thermal activation of the samples, thus further confirming the formation of a Pt, Cu alloy. Indeed, Pt, Cu alloys have been reported to form upon annealing to temperatures above 550 K of Cu epitaxially grown on Pt(111) surfaces [35].

Reported in Fig. 8 is the catalytic behavior of this sample in comparison with that of 1Pt–15Ba during NO_x storage–reduction tests at different reaction temperatures and before and after hydrothermal treatment. Although the addition of Cu slightly decreases the activity of the fresh sample in NO_x storage–reduction with respect to the 1Pt–HT (compare Fig. 7 and 8), 1Pt–Cu/HT shows significantly better NO_xSR performances than both 1Pt/HT and 1Pt–15Ba. At 300 and 400 °C the mean NO_x conversion in 1Pt–Cu/HT after hydrothermal treatment is about 50% higher than that of 1Pt–15Ba after similar treatment. At 500 °C the activity of 1Pt–Cu/HT is lower than that of 1Pt–15Ba, although activity can be promoted by adding metal alkaline oxides. The addition of Cu to 1Pt–15Ba (adding Cu before the Pt addition using a methodology similar to that

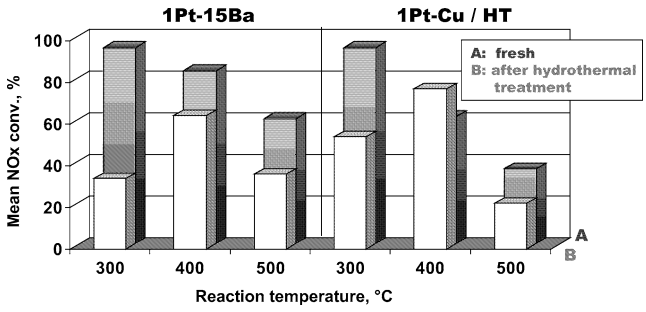

Fig. 8. Comparison of the mean NO_x conversion at different reaction temperatures for (i) 1Pt–Cu/HT [Pt (1%)–HT modified by the addition of 4% CuO prior to the loading of Pt] and (ii) 1Pt–15Ba [Pt (1%)–Ba (15%)/Al_2O_3] calcined at 650 °C before and after hydrothermal treatment.

used in preparing 1Pt–Cu/HT) instead lowers the activity before and after the hydrothermal treatment. For example, at 300 °C the NO_x mean conversion for fresh 1Pt–Cu (4%)–Ba (15%)/Al_2O_3 was about 60% and around 20% after hydrothermal treatment.

Control of the in situ phenomena of sintering of noble metal and NO_x storage–reduction catalysts by modification of the catalyst nanostructure is thus a promising direction to develop a new generation of catalysts for this application. Other research groups have recently found interesting results along this line by adding transition metals such as iron [36].

Hydrotalcite-based NO_xSR catalysts also show improved properties of resistance to deactivation by SO_2 [32,33] with respect to 1Pt–15Ba. Resistance to deactivation by SO_2 is a critical problem in the development of these catalysts [37].

In conclusion, the analysis of both the reaction mechanism and the nanostructure of the NO_xSR catalysts makes it possible to design samples with improved performances in the demanding conditions of application of these catalysts, i.e., continuous periodic cycling between reducing and oxidizing conditions, variations in reaction temperature from about 150 to over 650 °C, high and variable space velocities, presence of high concentrations of CO_2 and water, and presence of poisons such as SO_2. Further improvements are necessary, and a better understanding of the dynamic behavior at the nanoscale level and of the interaction of the different components forming the active site (noble metal, support, NO_x storage component(s), modifiers, and promoters).

3. Tuning metal particle size through metal–support interaction

The concept of the novel and unique physical and chemical properties of nanosized supported metals is well recognized in the literature [38–40]. Nanosized gold particles [38], for example, show reactivity properties very different from those of large particles, an example which is often used to emphasize the role of nanotechnology in the development of novel materials. Enhanced “composite” characteristics also may be obtained in nanocomposites consisting of nanometric metal particles dispersed in an oxide matrix. The physical (electrical, optical, magnetic) and mechanical properties of these nanocomposites are different from those of the analogous materials in which the metal is present as larger particles [41].

Nanosized metal particles can be obtained using a variety of methods, and usually the preparation methodology has a marked influence on the reactivity of these nanoparticles. It is also known that the nature of the support influences the size and stability of these metal particles, but a question often not considered in detail is how control of the electronic metal–support interaction affects the size of the supported metal particles. This question falls within the general problematics of nanostructured catalysts, because the reactivity and characteristics of the metal particle can be mod-

ified through changes in the environment around the particle and the metal–support interaction at a nanoscale level. The example discussed refers to modification of the reactivity and properties of Rh particles supported on zirconia for the decomposition of N_2O [42,43], but it is of more general validity in terms of both the nature of the noble metal and the type of support. The metal–support interaction discussed refers to the electronic interaction and change in the Fermi level, and is different from the SMSI (strong metal–support interaction) effect [44,45].

3.1. N_2O *decomposition*

The Kyoto Protocol of 1997 on greenhouse gas (GG) emissions stressed the necessity to control the emissions not only of CO_2, but also of methane and N_2O, which contribute 7 and 9%, respectively, to the global warming potential (GWP) (with reference to the CO_2 equivalent emissions, using GWP values for a 100-year time horizon) [4]. Only part of the sources of N_2O can be addressed by catalytic technologies. The more relevant cases are the off-gas from the synthesis and use of nitric acid and from combustion processes (especially of solid waste at temperatures below 1000 °C) [4]. In particular, the elimination of N_2O from the off-gas of nitric acid plants [46] is becoming an industrial problem of increasing importance. In these emissions, N_2O is present in a low concentration and together with other gas components such as H_2O, O_2, and NO. N_2O can be either catalytically decomposed or selectively reduced by adding a reductant (hydrocarbons such as propane or methane, or ammonia) [47,48]. Both solutions show advantages and disadvantages, but decomposition is preferable, when the rate is sufficiently high and the catalysts are not severely inhibited by the other components in the gas phase. This implies that it is necessary to develop improved catalysts for N_2O decomposition able to efficiently operate at temperatures below about 450 °C, because higher temperatures (such as those required by most of the commercial catalysts) make it economically preferable to use a selective reductant. Rh-on-zirconia-type catalysts show interesting properties as low temperature catalysts in N_2O decomposition [43,49,50].

3.2. Metal–support interaction and reactivity

The doping of zirconia with trivalent elements such as Ce^{3+}, Sb^{3+}, or Al^{3+} during the sol–gel preparation of the support makes it possible to obtain a further relevant promotion of the reactivity in N_2O decomposition [42]. However, while all trivalent dopants of zirconia significantly promote the activity of supported Rh in the decomposition of N_2O with respect to pure zirconia prepared with the same method or doped with a pentavalent ion, cerium and antimony show the more relevant effect. Although cerium ions are added as the trivalent ion during the preparation, they can be oxidized to Ce^{4+} during the calcination step. However, the effect being similar for all trivalent ions, although enhanced for Ce^{3+} and Sb^{3+}, the modification of the surface reactivity is associated with modification of the bulk zirconia properties induced by trivalent ions, more than modification of the surface properties. In agreement, if the trivalent ion is added by impregnation on preformed zirconia, it depresses activity instead of promoting activity [42]. The effects for various types of trivalent ions having different redox characteristics or electronic properties (Ce^{3+}, Sb^{3+}, Y^{3+}, and Al^{3+}) but analogous ionic radii are similar. This indicates that the promotion effect is related to a structural effect more than to redox or electronic properties specific to the doping agents.

In all cases, X-ray diffraction analysis shows the presence of a substitutional solid solution of the dopant in the tetragonal zirconia phase, at least for the low levels of doping (maximum 3 wt%) investigated [42].

The effect of the amount of Ce^{3+} dopant in zirconia on the properties of Rh–$Z(Ce_x)$ samples, where $x = 0$–3 wt%, is summarized in Fig. 9a. As an index of catalytic activity in the decomposition of N_2O in the presence of oxygen, the rate constant of N_2O depletion at 270 °C is reported in Fig. 9a [k_{N_2O}(270 °C)]. The rate constant was estimated assuming a first order rate equation and a plug-flow type reactor model, hypotheses that were both verified to be valid in the selected experimental conditions.

The amount of dopant has a volcano-type influence on the catalyst reactivity in the decomposition of N_2O, with a maximum in activity for a dopant concentration of around 1.3%, which corresponds to about a Zr^{4+}:Ce^{3+} = 1:0.01 molar ratio. An analogous trend was observed for the other dopants (Sb^{3+}, for example), with a maximum in good correspondence with that shown by cerium (Fig. 9a) on a molar basis. This further confirms that the effect primarily must be attributed to the substitution of a trivalent ion for Zr^{4+} more than to a specific role of the dopant itself.

The replacement of zirconium ions with a trivalent ion should induce the formation of point defects (oxygen vacancies) due to charge balance, but when the number of these defects is above a certain level, structural reconstruction to more ordered phases (or phases having extended defects such as shear-planes) is expected. It is thus reasonable that a maximum in catalytic reactivity is observed as a consequence of the change from a defective zirconia containing localized oxygen vacancies to a more ordered defective zirconia, such as when ordered shear planes form.

The presence of localized oxygen vacancies should also increase catalyst reducibility and thus a maximum in the plot of catalyst reducibility vs the amount of dopant is expected. To check this hypothesis, catalyst reducibility was analyzed by reducing the catalysts under mild and controlled conditions and determining the number of oxygen vacancies in the catalyst by reoxidation at room temperature with N_2O. The results as a function of the amount of dopant are also summarized in Fig. 9a, which reports the moles of N_2O necessary to reoxidize the catalyst at room temperature

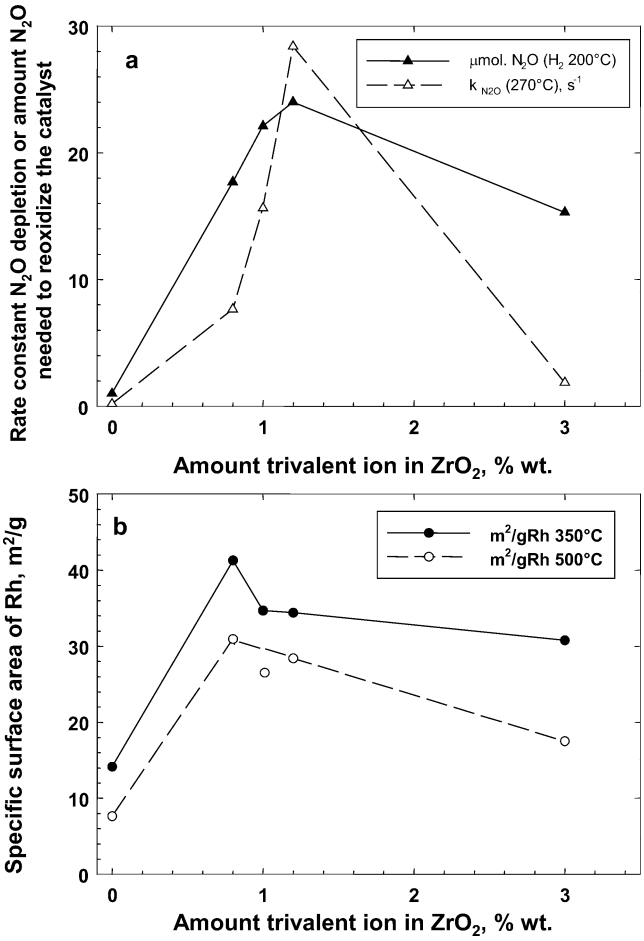

Fig. 9. (a) Effect of the amount of Ce^{3+} in tetragonal ZrO_2 on the amount of N_2O used to reoxidize the catalyst at r.t. after mild reduction at 200 °C with H_2, and rate constant of N_2O depletion at 270 °C in the presence of 6% O_2. (b) Specific surface area of Rh (m^2/gRh) determined by H_2 r.t. chemisorption after activation at 350 or 500 °C.

after controlled reduction with H_2 at 200 °C [mol N_2O (H_2 200 °C)].

There is a good parallel trend between the rate of N_2O depletion and the catalyst reducibility, which further supports the hypothesis that the stabilization of oxygen vacancies by controlled doping of zirconia will also stabilize oxygen vacancies at the Rh–zirconia interface. The presence of these oxygen vacancies, enhancing the effective removal of oxygen adatoms (formed by N_2O dissociation) from the Rh surface (rate-limiting step of the reaction) [43], leads to a parallel enhancement of the rate of N_2O dissociation, notwithstanding the fact that the oxygen concentration is around 1000 times higher than the N_2O concentration.

As a consequence of the hypothesis of the presence of oxygen vacancies at the Rh–zirconia interface increased stabilization of the Rh particles is expected. To verify this stabilization, the surface area of the metallic Rh particles after reduction with H_2 under controlled conditions at 350 and 500 °C was determined by a selective chemisorption technique (H_2 at r.t.). The results in terms of specific Rh surface area (m^2/g) after reduction at 350 or 500 °C (m^2/g Rh 350 or 500 °C, respectively) are also reported in Fig. 9b as a function of the amount of dopant.

A maximum in the specific surface area of metallic Rh with respect to the amount of dopant is also observed in this case, although the position of the maximum occurs at a slightly lower cerium concentration (around 0.8%). It is worth noting that the treatment with hydrogen under more severe conditions (500 °C) produced only limited sintering of the Rh particles, indicating their strong stabilization due to the presence of the hypothesized interfacial oxygen vacancies. While in Rh on pure zirconia the H_2 treatment at 500 °C reduced the Rh surface area to about 50% with respect to the treatment at 350 °C, the reduction is only 20% in the Rh–Z (Ce0.8) sample, confirming the enhanced stability towards sintering of the noble metal of doped zirconia samples.

The position of the maximum in the specific surface area of Rh particles for a different value of dopant concentration with respect to the maximum in the rate of N_2O depletion indicates that the two effects are distinct, although correlated, i.e., that the maximum in the rate of N_2O depletion is not due to simply a higher specific surface area of the Rh particles. This was confirmed by analyzing the change in reactivity and catalyst properties as a function of the Rh loading.

In conclusion, this example shows that the addition of small amounts of the trivalent ion, inducing controlled oxygen vacancies in the zirconia support, is a means of tuning the metal particle size through metal–support interaction and of promoting surface reactivity in N_2O decomposition even in the presence of a concentration of O_2 two to three orders of magnitude higher than that of N_2O.

4. Conclusions and perspectives

Catalysis was familiar with the concept of nanostructure much earlier than the start of current interest in nanotechnologies and nanoscience. It is now clear that the concept of catalyst nanostructure in terms of an intermediate level between the molecular level at a single site and the macrolevel of overall catalyst structure can be a useful unifying concept for several aspects of catalysis, some of which are well recognized and others less so, such as those related to how the nanoarchitecture of the active sites and the related dynamic effects during catalytic reaction determine the performance, or how the nanoenvironment around the active sites influences the reactivity. There are several recent results which evidence, for example, that by controlling the hydrophobicity of the support around an anchored complex or by including the active sites in ordered nanocavities it is possible to control the selectivity and/or activity. This finds application in areas ranging from fine chemical synthesis to reactions for environmental protection.

In the control of nitrogen oxides, the concept of nanostructured catalysts can be a possibility to approach the tailoring of the catalysts or the design of novel materials. Discus-

sion have been limited here to two specific examples: (i) the development of catalysts based on hydrotalcite precursors as novel NO_x storage–reduction materials with improved hydrothermal resistance and (ii) the control of metal particle size by creating oxygen vacancies in the zirconia support in order to develop more active catalysts in N_2O decomposition.

Also in the reduction of NO_x in stationary or mobile sources, the concept of nanostructured catalysts find a wide range of applications. Current commercial catalysts for these applications are based on multilayered materials with graduated catalyst composition in order to optimize catalyst performances and stability. The last generation of three-way catalysts for NO_x conversion in autoexhaust emissions are based on La- or Ba-doped alumina (doping is necessary to improve hydrothermal stability of alumina) on which the oxygen storage component (ceria–zirconia) and noble metals (Pt, Rh, and/or Pd) are supported. The optimal interaction between these three catalyst components or in other words the nanoarchitecture of the catalyst is the key to maximize performances under the rapid transients in feed composition present in autoexhaust emission and to realize the high thermal and mechanical stability required from the application.

The concept of controlling the nanostructure of the catalysts finds application in a more wide range of situations of interest for catalytic technologies, but is it of special relevance in the area of applications to environment protection. This research topic of catalysis is one having the faster growth in interest over the last decade.

The preparation of nanomaterials with controlled morphology and size attracted a large research interest, because particles at a nanoscale level can show different reactivity properties. However, nanosized particles have also a large perimeter area of contact with other phases such as of co-catalyst components or a support oxide. This area of contact is often the determining aspect of the reactivity. The examples discussed in this contribution show that the support may have a direct specific role in the reaction mechanism, in the dynamic of transformation of the catalyst during the reaction and in determining catalyst stability.

Over the past 10 years, it was a progressive accumulation of evidence showing that during the catalytic reaction often there is a continuous dynamic reconstructuring of the catalyst. These evidences indicate that in describing the catalytic behavior the attention should be shifted from the molecular level only (reaction at a defined active site) to the nanostructure level (the region around the active site(s)) and its dynamic of transformation during the catalytic reaction.

The catalysis for the control of nitrogen oxide emissions was one of the first areas to recognize the relevance of this supramolecular architecture of the solid catalysts in determining catalyst performances and stability, in order to develop, for example, autoexhaust treatment catalysts efficiently operating under rapid transients in feed composition. However, this is a more general concept for catalysis and one of the directions of research also in other areas such as that of selective oxidation catalysts for which the concept of "living active surface" was introduced recently [51].

Today, several in situ characterization techniques are available which allow a better understanding and demonstration of the concepts outlined above, although the time resolution is a limit. Often what is considered "stationary" behavior is simply a dynamic situation having a frequency of periodic changes too fast to be detected. New faster in situ techniques are expected in the next years which will be really greatly improve our understanding of the dynamics of catalysis at a molecular and nanoscale level. Theoretical methods should also try to make an effort towards a better understanding of the dynamic behavior at a nanoscale level instead of focusing activity to the active site level only.

The possibility of controlling nanostructure around the active sites is one of the key aspects and opportunities which differentiate catalysis on solid surfaces from homogeneous catalysis and which make it possible to realize complex reactions requiring multifunctional behavior or catalytic transformations not having a counterpart in homogeneous catalysis.

Understanding the catalyst nanostructure is also relevant closing the gap between catalysis by enzymes and by solid materials. Cu zeolites, originally developed for the decomposition or selective reduction of NO, were one of the first catalytic example for which the concept of "solid enzyme" was introduced to explain and model the catalytic behavior [52]. Later, this concept was used in several other examples.

The understanding of the nanostructure level of catalysts and of its dynamic behavior during reaction is thus an area which is expected to give a major contribution to a wider application of catalysis also outside the traditional areas of chemical and refinery applications and especially to the field of catalytic technologies for environmental protection and improvement of the quality of life.

Acknowledgment

This work was carried out with the financial support of the COFIN2000 project "Catalysts for the Removal of Nitrogen Oxides in Lean Burn Engine Emissions."

References

[1] G. Ertl, H. Knözinger, J. Weitkamp (Eds.), Environmental Catalysis, Wiley–VCH, Weinheim, Germany, 1999.
[2] G. Centi, P. Ciambelli, S. Perathoner, P. Russo, Catal. Today 75 (2002) 3.
[3] J. Levec, A. Pintar, Catal. Today 24 (1995) 51.
[4] G. Centi, S. Perathoner, F. Vazzana, CHEMTECH 29 (1999) 48.
[5] A. Fritz, V. Pitchon, Appl. Catal. B Environ. 13 (1997) 1.
[6] B.A.A.L. Van Setten, M. Makkee, J.A. Moulijn, Catal. Rev. Sci. Eng. 43 (2001) 489.

[7] G. Martino, Stud. Surf. Sci. Catal. 130 (2000) 83.
[8] M. Misono, Toyota Techn. Rev. 44 (1995) 4.
[9] A. Cybulski, J.A. Moulijn (Eds.), Structured Catalysts and Reactors, in: Chemical Industries, Vol. 71, Dekker, New York, 1998.
[10] F. Kapteijn, J.J. Heiszwolf, T.A. Nijhuis, J.A. Moulijn, CATTECH 3 (1999) 24.
[11] Yu. Matatov-Meytal, M. Sheintuch, Appl. Catal. A Gen. 231 (2002) 1.
[12] J.Y. Ying, AiChE J. 46 (2000) 1902.
[13] G. Centi, S. Perathoner, in: Proceedings CAMURE4 (Lausanne, Switzerland, Sept. 2002), Catal. Today (2002), in press.
[14] S. Matsumoto, CATTECH 4 (2001) 102.
[15] K. Katoh, T. Kihara, T. Asanuma, M. Gotoh, N. Shibagaki, Toyota Tech. Rev. 44 (1995) 27.
[16] S. Matsumoto, Y. Ikeda, H. Suzuki, M. Ogai, N. Miyoshi, Appl. Catal. B Environ. 25 (2000) 115.
[17] S. Erkfeldt, M. Larsson, H. Hedblom, M. Skoglundh, SAE Paper SP 1476 (1999).
[18] A. Amberntsson, B. Westerberg, P. Engstrom, E. Fridell, Stud. Surf. Sci. Catal. 126 (1999) 317.
[19] E. Fridell, H. Persson, B. Westerberg, L. Olsson, M. Skoglundh, Catal. Lett. 66 (2000) 71.
[20] J.A. Anderson, A.J. Paterson, M. Fernandez-Garcia, Stud. Surf. Sci. Catal. 130 (2000) 1331.
[21] P. Engstrom, A. Amberntsson, M. Skoglundh, E. Fridell, G. Smedler, Appl. Catal. B Environ. 22 (1999) L241.
[22] S. Balcon, C. Potvin, L. Salin, J.F. Tempere, G. Djéga-Mariadassou, Catal. Lett. 60 (1999) 39.
[23] E. Fridell, M. Skoglundh, B. Westerberg, S. Johansson, J. Catal. 183 (1999) 196.
[24] F. Rodrigues, L. Juste, C. Potvin, J.F. Tempere, G. Blanchard, G. Djéga-Mariadassou, Catal. Lett. 72 (2001) 59.
[25] K.I. Hadjiivanov, Catal. Rev. Sci. Eng. 42 (2000) 71.
[26] P.J. Schmitz, R.J. Baird, J. Phys. Chem. B 106 (2002) 4172.
[27] A.J. Paterson, D.J. Rosenberg, J.A. Anderson, Stud. Surf. Sci. Catal. 138 (2001) 429.
[28] F. Prinetto, G. Ghiotti, I. Nova, L. Lietti, E. Tronconi, P. Forzatti, J. Phys. Chem. B 105 (2001) 12732.
[29] L. Lietti, P. Forzatti, I. Nova, E. Tronconi, J. Catal. 204 (2001) 175.
[30] G. Centi, G. Fornasari, G. Gobbi, M. Livi, F. Trifirò, A. Vaccari, Catal. Today 73 (2002) 287.
[31] G. Fornasari, M. Livi, F. Trifirò, A. Vaccari, L. Balduzzi, F. Prinetto, G. Ghiotti, G. Centi, Catal. Today 75 (2002) 421.
[32] F. Cavani, F. Trifirò, A. Vaccari, Catal. Today 11 (1991) 173.
[33] A.J. Marchi, C.R. Apesteguia, Appl. Clay Sci. 13 (1998) 35.
[34] N.A. Sokolova, A.P. Barkova, D.B. Furman, V.Yu. Borokov, V.B. Kazanski, Kinet. Katal. 36 (1995) 434, and references therein.
[35] J.A. Rodriguez, C.M. Truong, D.W. Goodman, J. Chem. Phys. 96 (1992) 7814.
[36] K. Yamazaki, T. Suzuki, N. Takahashi, K. Yokota, M. Sugiura, Appl. Catal. B Environ. 30 (2001) 459.
[37] H. Hirata, I. Hachisuka, Y. Ikeda, S. Tsuji, S. Matsumoto, Top. Catal. 16/17 (2001) 145.
[38] (a) M. Haruta, Catal. Today 36 (1997) 153;
(b) M. Haruta, Stud. Surf. Sci. Catal. 110 (1997) 123.
[39] A.I. Kozlov, A.P. Kozlova, H. Liu, Y. Iwasawa, Appl. Catal. A Gen. 182 (1999) 9.
[40] C.C. Chusuei, X. Lai, K. Luo, D.W. Goodman, Top. Catal. 14 (2001) 71.
[41] Ch. Laurent, A. Rousset, Key Eng. Mater. 108–110 (1995) 405.
[42] G. Centi, B. Panzacchi, S. Perathoner, F. Pinna, Stud. Surf. Sci. Catal. 130 (2000) 2273.
[43] G. Centi, L. dall'Olio, S. Perathoner, Appl. Catal. A Gen. 194–195 (2000) 79.
[44] B. Coq, in: Metal–Ligand Interactions in Chemistry, Physics and Biology, in: NATO Science Series, Series C: Mathematical and Physical Sciences, Vol. 546, 2000, p. 49.
[45] K. Hayek, R. Kramer, Z. Paal, Appl. Catal. A Gen. 162 (1997) 1.
[46] R.W. van den Brink, S. Booneveld, M.J.F.M. Verhaak, F.A. de Bruijn, Catal. Today 75 (2002) 227.
[47] G. Centi, F. Vazzana, Catal. Today 53 (1999) 683.
[48] F. Kapteijn, J. Rodriguez-Morasol, J.A. Moulijn, Appl. Catal. B Environ. 9 (1996) 25.
[49] G. Centi, L. dall'Olio, S. Perathoner, J. Catal. 194 (2000) 130.
[50] G. Centi, S. Perathoner, F. Vazzana, M. Marella, M. Tommaselli, M. Mantegazza, Adv. Environ. Res. 4/4 (2000) 325.
[51] G. Centi, F. Cavani, F. Trifirò, in: M.V. Twigg, M.S. Spencer (Eds.), Selective Oxidation by Heterogeneous Catalysis. Recent Developments, in: Fundamental and Applied Catalysis Series, Kluwer/Plenum, New York/London, 2001.
[52] G. Centi, S. Perathoner, Appl. Catal. A Gen. 132 (1995) 179.